Photosubstitution and photoreduction of a diazido platinum(IV) anticancer complex

Huayun Shi,[†a] Christian Ward-Deitrich,[†b] Fortuna Ponte,[c] Emilia Sicilia,*[c] Heidi Goenaga-Infante,*[b] Peter J Sadler*[a]

[a] Department of Chemistry, University of Warwick, Coventry CV4 7AL, UK

[b] LGC Limited, National Measurement Laboratory (NML), Queens Road, Teddington, Middlesex TW11 0LY, UK

[c] Department of Chemistry and Chemical Technologies, University of Calabria, via Pietro Bucci, 87036 Arcavacata di Rende, Cs, Italy

[†] Joint first authors

* Corresponding authors

Content

Experimental section

Caution! Heavy metal azides can be shock-sensitive. All experiments in this paper were carried out under minimal light exposure with care and no problem was encountered during the work reported here.

Materials and instruments.

Materials.

FM-190 was prepared using the modified synthetic route reported previously.[1]

HPLC grade acetonitrile was from Sigma-Aldrich, HPLC grade methanol (CH_3OH) was from Fisher and formic acid (FA) were purchased from Fluka and used as received. Mobile phases used for all HPLC experiments are 0.1% FA in Water (solvent A) and 0.1% FA in CH_3OH (solvent B) unless stated otherwise.

Freeze dried human plasma was from Sigma-Aldrich, 5 mL MilliQ Water was added to make the reconstituted plasma. Dulbecco's Phosphate-buffered saline (PBS) was from Biowest.

Platinum (1001 ± 12 mg/L TraceCERT® platinum in 5% v/v hydrochloric acid) was purchased from Inorganic Ventures and used as standard for calibration of platinum by ICP-MS.

Instruments.

Column: Agilent ZORBAX Eclipse XDB-C18 column (250×4.6 mm, 5 μm, flow rate: 1 mL/min)

HPLC-UV: Agilent 1100 HPLC

HPLC-MS: Bruker Amazon X mass spectrometry connected online to an Agilent 1260 HPLC

HPLC-ICP-MS: Agilent 8800 Triple Quad ICP-MS connected online to an Agilent 1200 HPLC

ICP-MS: Agilent 7900 series ICP-MS

HR-MS: Bruker Compact Q-TOF

LED light sources (BASETech model no. SP-GU10, 230 V~50 Hz, 64 mW/cm^2) with λ_{max} = 463 nm is used for irradiation. Samples were placed in a distance of 3 cm from light source.

Sample preparation.

Dark and photoactivated samples in MilliQ water.

FM-190 was dissolved in MilliQ water to prepare a 1 mM stock solution. The stock solution was then further diluted in MilliQ water to make 1 mL samples aliquots with different concentrations for HPLC-UV, LC-MS and HPLC-ICP-MS analysis. The dark samples were analysed directly, while the photoactivated samples were irradiated with blue light (463 nm) for 1 h at 25°C.

Dark and photoactivated samples in plasma and PBS.

FM-190 was dissolved in PBS, then 40 μL of the PBS solution of **FM-190** (5x of final concentration) were diluted with 160 μL Plasma or 160 μL PBS, respectively. The resulting solutions were incubated at 37°C for 1 h in the dark. The dark sample was kept in the dark for an additional 1 h; while the photoactivated samples were irradiated with blue light (463 nm) at 25°C.

Extraction from plasma. Two protocols were used to extract the Pt compounds from plasma. **Acetonitrile protocol.** 200 µL acetonitrile was added to the sample solution, followed by centrifugation at 13,000 rpm for 30 min. The supernatant (300 µL) was transferred into a new vial, remaining acetonitrile was evaporated in a fumehood, and samples were then freeze dried. For final dilution it was resolubilised with 1500 or 750 µL MilliQ water to, make 10x or 5x diluted solutions for HPLC-ICP-MS and LC-MS analysis, respectively. The solution was transferred to Eppendorf vials, then centrifuged at 15,000 rpm for 10 min. The supernatant was filtered before HPLC injection.

Centrifugal filter protocol. The sample was centrifuged in a centrifugal filter unit (MWCO 5,000 Da) at 13,000 rpm for 30 min, then 100 µL of supernatant was transferred to a new vial, then freeze dried. 1000 or 500 µL MilliQ water was added to make a 10x or 5x diluted solution for HPLC-ICP-MS and LC-MS analysis, respectively. The solution was filtered before HPLC injection.

Isolation of photoactivated products by HPLC for HR-MS.

A 100 µM **FM-190** solution in MilliQ water was irradiated with blue light (463 nm) for 1 h at 25°C. A 50 µL portion was submitted to HPLC separation, using an Agilent 1100 HPLC equipped with an Agilent ZORBAX Eclipse XDB-C18 column (250×4.6 mm, 5 µm, flow rate: 1 mL/min), with gradients of 0.1% FA in water (solvent A) and 0.1% FA in methanol (solvent B) according to Method-8 (**Table S2**). The eluent from 8.4 min to 10 min was collected for 8 injections combined and freeze dried. The residue was redissolved in 400 µL MilliQ water for HR-MS analysis.

Analytical procedures.

HPLC-UV, HPLC-ICP-MS and HPLC-MS.

HPLC-UV, HPLC-ICP-MS, and HPLC-MS experiments were carried out using an Agilent 1100 (HPLC-UV), Agilent 1200 (HPLC-ICP-MS), or Agilent 1260 HPLC (HPLC-MS) system equipped with a binary pump, degasser, thermostatted autosampler (for HPLC-UV, manual injection was used instead) and column compartment, and a UV detector. The injection volume was 50 µL solution for each HPLC system. Separation of the different Pt-species was achieved using an Agilent ZORBAX Eclipse XDB-C18 column (250×4.6 mm, 5 µm). In ICP-MS, exposure to organic solvents at high concentration may extinguish or severely alter the stability of plasma.[2–4] In addition, carbon from the organic solvents leads to deposits on the interface cones, which causes clogging of the ICP-MS cones and a rapid loss of sensitivity. To reduce the carbon content and create a more stable plasma, methanol + 0.1% FA rather than the more commonly used acetonitrile was used as the HPLC mobile phase (B), accompanied by water + 0.1% FA (mobile phase A). Furthermore, the gradient elution was optimised to ensure all Pt species in the samples could be monitored by HPLC-ICP-MS with a ratio of the organic solvent lower than 8%. Thus, mobile phase A was 100% water with 0.1% (v/v) FA and mobile phase B was 100% methanol with 0.1% (v/v) FA. Elution was achieved using an optimised gradient as shown in **Tables S1**, **S2** and **S6**. The UV signal at 254 nm was also monitored.

For HPLC-ICP-MS, an Agilent 1200 HPLC system was coupled to an Agilent 8800-QQQ-ICP-MS. The system was equipped with a switching valve, and an online column washing step was included by diverting the high solvent containing eluent away from the plasma into the waste. The outlet of the column was connected directly via PEEK tubing to the ICP-MS equipped with a MicroMist nebuliser, a Peltier-cooled (2 °C) Scott spray chamber and nickel cones. The ICP-MS was tuned daily for optimised conditions. The Pt isotopes were monitored in standard mode (no gas) and a dwell time of 0.2 s for all isotopes. For general ICP-MS operating conditions see **Table S2**.

An Agilent 1260 system was coupled with a Bruker Amazon X mass spectrometry for HPLC-MS

analysis. The system was operated in positive mode with a mass range of m/z 50-3000. The detector was optimised between different batches of samples. Therefore, a slight mass shift is observed from calculated value due to systemic error, which is corrected using **FM-190**+Na^+ (493.98) as a reference peak/signal.

ICP-MS.

Total Pt in **FM-190** solutions was determined by external calibration using an Agilent 7900 series ICP-MS. The calibration curve is obtained using standards in a range of 0-500 ppb made up in 3.6% HNO_3.

The **FM-190** stock solution (ca. 1 µM) in MilliQ water was diluted by 10x in 3.6% HNO_3 to get a final volume of 3 mL for ICP-MS analysis.

The stock solution of **FM-190** (ca. 50 µM) use for the plasma and PBS experiments was diluted by 10x in 3.6% HNO_3. This solution was then further diluted by 10x in 3.6% HNO_3 to obtain 5 mL solution for ICP-MS analysis.

DFT Calculations.

All calculations were carried out using the Gaussian16 program suite,[5] in the framework of the density Density Functional Theory (DFT) and its time-dependent density functional linear response formulation (TDDFT). The hybrid B3LYP functional coupled with the D3 Grimme's dispersion correction for nonbonding interactions was adopted[6–8] along with the SDD pseudo-potential for the Pt atom and the associated valence basis set,[9] For the rest of atoms the 6-31G* basis set was employed. The impact of the aqueous solvent was taken into account by considering the dielectric constant of 78.4, within the Tomasi implicit polarisable continuum model[10] as implemented in Gaussian16. The electronic spectra were obtained within the nonequilibrium time-dependent TDDFT approach, as vertical electronic excitations on the ground-state structure, at the same level of theory used for the full geometrical optimizations, by performing 150 electronic excitations. Such a computational protocol was selected on the basis of the outcomes of a preliminary benchmark study, considering the performance of several exchange-correlation functionals, in reproducing the absorption spectrum of the complex compared with that experimentally detected. B3LYP-D3,[6–8] CAM-B3LYP,[11] PBE,[12] PBE0,[13] M05,[14] M06,[15] M06L[16] functionals were tested for this purpose. On the basis of the agreement between theoretical and experimental values of the absorption wavelengths, the B3LYP functional was selected. The optimized structures of all the excited states, below the bright state, potentially involved in the complex photoactivation were primarily explored using the TDDFT in a condensed phase and then, within the unrestricted Kohn–Sham formalism (UKS).[17,18] To establish the probability for a triplet state to be populated through intersystem spin crossing (ISC), spin-orbit matrix elements were calculated using the SOC-TD-DFT approach implemented in Orca code.[19,20] SOC values were calculated according to Equation 1:

$$SOC_{nm} = \sqrt{\sum_i \left|\langle \psi_{S_n} | \hat{H}_{SO} | \psi_{T_{i,m}} \rangle\right|^2}; \qquad i = x, y, z \qquad (1)$$

Where $\hat{H}_{SO}$ is the spin-orbit Hamiltonian with effective nuclear charge. Relativistic corrections were obtained by the zeroth order regular approximation (ZORA). ZORA-DEF2-SVP and SARC-ZORA-SVP basis sets were used for the main and metal atoms, respectively. The RIJCOSX approximations were introduced to speed up the calculations' time, as suggested in the ORCA manual and very tight SCF convergence and a very large grid (Lebedev 770 points) were set for such calculations.

The optimization of all the stationary points as minima or transition states along the singlet free energy

profile was performed at the same level of theory. Frequency calculation was also carried out, to explore and confirm the nature of the intercepted stationary points and to calculate zero-point energy (ZPE) corrections. Moreover, the intercepted transition states were carefully checked to be properly connected to the correct minima by the Intrinsic Reaction Coordinate algorithm.[21,22]

All the K_a values were calculated considering the free energy change (G) that accompanies the deprotonation reaction:

$$AH^n + H_2O \rightarrow A^{n-1} + H_3O^+ \qquad (2)$$

where n is the charge of the generic complex AH. Using eqn (2), the pK_a of the complex can be evaluated using the following equation:

$$pK_a = -1.74 + 0.733\Delta G \qquad (3)$$

where the constant 0.733 = 1/RTln10, in kcal mol^{-1}.

Table S1. Optimisation of HPLC-ICP-MS methodology for **FM-190**.

HPLC chromatography	
HPLC instrument	Agilent 1100
Column	Agilent ZORBAX Eclipse XDB-C18 column (250x4.6 mm, 5 µm)
Flow rate	1 mL/min
Injection volume	50 µL
Detection wavelength	254 nm
Mobile Phase	Water + 0.1% FA (A); Methanol + 0.1% FA (B)

Time/min	Method-1 %B	Time/min	Method-2 %B	Time/min	Method-3 %B	Time/min	Method-4 %B
0	2	0	2	0	2	0	2
30	80	30	30	30	20	30	10
35	80	35	30	35	20	35	10
36	2	36	2	36	2	36	2
41	2	41	2	41	2	41	2
Time/min	Method-5 %B	Time/min	Method-6 %B	Time/min	Method-7 %B		
0	2	0	2	0	2		
20	10	10	8	10	5		
25	10	15	8	15	5		
26	2	16	2	16	2		
41	2	21	2	21	2		

Table S2. Optimal HPLC-ICP-MS and LC-MS methods for **FM-190** analysis.

HPLC instrument	Agilent 1200
Column	Agilent ZORBAX Eclipse XDB-C18 column (250x4.6 mm, 5 μm)
Flow rate	1 mL/min
Injection volume	50 μL
Detection wavelength	254 nm
Mobile Phase	Water + 0.1% FA (A); Methanol + 0.1% FA (B)
ICP instrument	Agilent 8800 Triple Quad
ICP-MS cone	Nickel
Mode	No gas
Dwell time	0.2 s
Pt m/z	194, 195, 196
Mass spectrometry	Bruker Amazon X

Time/min	Method-7 %B	Time/min	Method-8 %B
0	2	0	2
10	5	10	5
15	5	18	5
16	2	18.01	80[a]
21	2	23	80[a]
		24	2[a]
		29	2[a]

[a] For HPLC-ICP-MS, 80% Mobile phase B containing elution did not enter the ICP-MS, and was directed to the solvent waste.

Table S3. ^{195}Pt signal peak areas of **FM-190** at varied concentrations in MilliQ water in the dark obtained by HPLC-ICP-MS.

	Concentration Peak area/ratio							
	764.8 nM		45.9 nM		9.2 nM		4.6 nM	
Retention time/min[a]	Area	Ratio/%	Area	Ratio/%	Area	Ratio/%	Area	Ratio/%
4.55	120	0.065	0	0	0	0	0	0
8.76	89	0.048	0	0	0	0	0	0
14.10	184652	99.89	9714	100	2065	100	1046	100
Sum of peak areas	184861	100	9714	100	2065	100	1046	100

[a] Retention time refers to that in the ^{195}Pt peaks in **Figure 2**.

Table S4. ^{195}Pt signal peak areas of **FM-190** at varied concentration in MilliQ water after irradiation with blue light (463 nm, 1 h) obtained by HPLC-ICP-MS.

Concentration	764.8 nM		764.8 nM-after 24 h		45.9 nM		4.6 nM	
Retention time/min[a]	Area	Ratio/%	Area	Ratio/%	Area	Ratio/%	Area	Ratio/%
2.88	1752	0.853	1779	0.90	188	1.692	147	8.714
3.66	28382	13.81	32747	16.59	1051	9.460	164	9.721
4.61	17468	8.500	16408	8.31	6869	61.82	860	50.98
6.82	61139	29.75	56533	28.65	139	1.251	60	3.557
8.89	38823	18.89	36742	18.62	1731	15.579	263	15.59
11.27	28504	13.87	26151	13.25	0	0	0	0
14.16	16689	8.121	26990	13.68	1133	10.20	193	11.44
14.86	12750	6.204	0	0	0	0	0	0
Sum of peak areas	205507	100	197350	100	11111	100	1687	100

[a] Retention time refers to that in the ^{195}Pt peaks in **Figure 3**.

Table S5. Mass and corresponding expected structures of photoproducts of **FM-190** (31.8 μM) determined by LC-MS (mobile phase: water and methanol).

Retention time/min[a]	Peak	Mass calculated	Mass found	Formula
3.5	a	444.05	443.95; 865.04	$[\{Pt^{IV}(py)_2(OH)_4\}+Na]^+$
6.1	b	863.09	863.04	$[\{Pt^{IV}(py)_2(OH)_3\}_2(\mu\text{-}O_2)+Na]^+$
8.4	c	469.06	468.95; 915.04	$[\{Pt^{IV}(py)_2(N_3)(OH)_3\}+Na]^+$
10.2	d	473.05	472.94; 923.01	$[\{Pt^{III}(py)_2(HCOO)(OH)_2(H_2O)\}+Na]^+$
13.3	e	489.05	488.94	$[\{Pt^{III}(py)_2(HCOO)_3\}+H]^+$
13.9	**FM-190**	494.06	493.98; 965.05	$[\{Pt^{IV}(py)_2(OH)_2(N_3)_2\}+Na]^+$

[a] Retention time refers to that in the LC-UV signals in **Figure S4**.

Table S6. LC-MS method for **FM-190** analysis in aqueous solution.

HPLC instrument	Agilent 1260
Column	Agilent ZORBAX Eclipse XDB-C18 column (250x4.6 mm, 5 µm)
Flow rate	1 mL/min
Injection volume	50 µL
Detection wavelength	254 nm
Mobile Phase	Water + 0.1% FA (A); Acetonitrile + 0.1% FA (B)
Mass spectrometry	Bruker Amazon X

Time/min	Method-9 %B	Time/min	Method-10 %B
0	2	0	2
10	5	10	5
15	5	18	5
16	2	18.01	80
21	2	23	80
		24	2
		29	2

Table S7. Mass and corresponding expected structures of photoproducts of **FM-190** (50 µM) determined by LC-MS (mobile phase: water and acetonitrile).

Retention time/min[a]	Peak	Mass calculated	Mass found	Formula
3.2	α	444.05	443.95; 865.03	$[\{Pt^{IV}(py)_2(OH)_4\}+Na]^+$
3.7	β	863.09	862.99	$[\{Pt^{IV}(py)_2(OH)_3\}_2(\mu\text{-}O_2)+Na]^+$
6.2	γ	469.06	468.96; 915.01	$[\{Pt^{IV}(py)_2(N_3)(OH)_3\}+Na]^+$
7.5	δ	473.05	472.93; 922.97	$[\{Pt^{III}(py)_2(HCOO)(OH)_2(H_2O)\}+Na]^+$
9.6	ε	489.05	488.94	$[\{Pt^{III}(py)_2(py)_2(HCOO)_3\}+H]^+$
9.8	**FM-190**	494.06	493.98; 965.03	$[\{Pt^{IV}(py)_2(OH)_2(N_3)_2\}+Na]^+$

[a] Retention time refers to that in the LC-UV signals in **Figure S7**.

Table S8. TD-DFT benchmark for **FM-190** on the structure optimised at B3LYP-D3/6-31G* level in water implicit solvent.

Functional	State	λ	*f*	MO contribution
B3LYP-D3	S1	478	0.0000	H→L 98%
	S3	394	0.0046	H-2→L 99%
	S7	300	0.3610	H-3→L 81%
CAMB3LYP	S1	435	0.0000	H→L 94%
	S2	358	0.0059	H-1→L 88%
	S7	283	0.4548	H-2→L 89%
PBE	S1	546	0.0000	H→L 99%
	S3	445	0.0022	H-2→L 99%
	S7	395	0.0331	H-1→L+2 98%
	S28	293	0.2790	H-9→L 57%, H-3→L 31%,
PBE0	S1	468	0.0000	H→L 98%
	S3	393	0.0051	H-1→L 97%
	S7	294	0.4060	H-3→L 86%
M05	S1	493	0.0000	H→L 98%
	S3	398	0.0045	H-2→L 96%
	S8	301	0.3817	H-3→L 82%
M06	S1	494	0.0000	H→L 98%
	S3	400	0.0046	H-2→L 95%
	S8	305	0.3805	H-3→L 83%
M06L	S1	507	0.0000	H→L 95%
	S3	421	0.0030	H-2→L 100%
	S13	320	0.1439	H-3→L 46%, H-3→L+1 46%,
	S26	283	0.2104	H-1→L+5 42%, H-3→L 21%

Table S9. Excitation energies (ΔE, eV), absorption wavelength (λ, nm), oscillator strength (*f*), and MO contribution (%) for **FM-190** selected transitions.

Transition	**ΔE**	**λ**	***f***	**MO contribution**[a]	**Theoretical Assignment**[b]
Tr1	2.59	478	0.0000	H→L 98%	LMCT(30.9%), LC(25.0%), LLCT(29.8%)
Tr2	3.15	394	0.0046	H-2→L 99%	LMCT(35.0%), LLCT(33.8%), LC(30.2%)
Tr3	4.13	300	0.3610	H-3→L 81%	LLCT(39.8%), LMCT(35.3%), LC(22.3%)
Tr4	4.16	298	0.0056	H→L+2 98%	LLCT(84.8%)
Tr5	4.17	297	0.0097	H-2→L+1 98%	LMCT(50.5%), LLCT(47.4%)
Tr6	4.37	284	0.0682	H-3→L+1 90%	LMCT(48.4%), LLCT(44.5%)
Tr7	4.47	277	0.0056	H-7→LUMO 61%, H-1→L+2 23%	LLCT(56.3%), LMCT(30.7%)
Tr8	4.70	264	0.0130	H-4→L+1 69%, H-7→L+1 21%	LMCT(47.9%), LLCT(40.7%)
Tr9	4.73	262	0.0716	H-9→L 87%	LLCT(54.9%), LMCT(35.7%)
Tr10	4.84	256	0.0087	H-2→L+3 98%	LLCT(93.5%)

TheoDORE software together with NTO plots were used for assigning character of states. [a] For MO, only contributions larger than 22% are reported. [b] For theoretical assignment, only contributions larger than 22% are reported.

Table S10. Excitation energies (ΔE, eV), absorption wavelength (λ, nm), oscillator strength (*f*), and MO contribution (%) for **FM-190** selected singlet states.

State	ΔE	λ	*f*	MO contribution[a]	Theoretical Assignment[b]
S1	2.59	478	0.0000	H→L 98%	LMCT(30.9%), LC(25.0%), LLCT(29.8%)
S2	3.08	403	0.0000	H-1→L 99%	LLCT(40.2%), LMCT(27.2%), LC(22.0%)
S3	3.15	394	0.0046	H-2→L 98%	LMCT(35.0%), LLCT(33.8%), LC(30.2%)

TheoDORE software together with NTO plots were used for assigning states character. [a] For MO only contributions larger than 22% are reported. [b] For theoretical assignment, only contributions larger than 22% are reported.

Table S11. Excitation energies (ΔE, eV), absorption wavelength (λ, nm) and MO contribution (%) for **FM-190** selected triplet states.

State	ΔE	λ	MO contribution[a]	Theoretical Assignment[b]
T1	2.26	549	H→L 98%	LMCT(29.7%), LC(26.2%), LLCT(25.7%)
T2	2.75	451	H-1→L 86%	LLCT(31.5%), LMCT(25.9%), LCT(21.4%)
T3	2.76	449	H-3→L 98%	LMCT(33.8%), LC(32.6%), LLCT(31.1%)
T4	2.84	437	H-2→L 95%	LMCT(35.0%), LC(34%), LLCT(30.6%)
T5	3.05	407	H-1→L+1 84%	LMCT(30.2%), LLCT(22.0%)

TheoDORE software together with NTO plots were used for assigning states character. [a] For MO, only contributions larger than 22% are reported. [b] For theoretical assignment, only contributions larger than 22% are reported.

Table S12. Spin orbit coupling constants, SOC, and adiabatic energy gap (in brackets), ΔE(S-T), calculated for **FM-190**.

$S_m \rightarrow T_n$		Tn				
		1	2	3	4	5
Sm	1	25.0 (0.33)				
	2	714.0 (0.82)	0.38 (0.33)	33.8 (0.32)	0.1 (0.24)	0.1 (0.03)
	3	0.1 (0.89)	35 (0.40)	0.0 (0.39)	2.2 (0.31)	14.6 (0.10)

Table S13. ^{195}Pt signal peak areas of **FM-190** (7756 nM) in plasma or PBS after 2 h incubation in the dark at 37°C obtained by HPLC-ICP-MS.

Retention time/min[a]	Plasma-dark Area	Ratio/%	PBS-dark Area	Ratio/%
2.00-7.23	2136	1.601	1079	0.765
8.86	483	0.362	228	0.162
10.66	231	0.173	113	0.080
11.58	181	0.136	205	0.145
14.24	130336	97.73	139490	98.85
Sum	133367	100	141115	100

[a] Retention time refers to that in the ^{195}Pt peaks in **Figure S11**. Pt species were extracted from solution by centrifugal filter unit (MWCO 5000) and diluted 10x with MilliQ water.

Table S14. ^{195}Pt signal peak areas of **FM-190** (7756 nM) in plasma after 2 h incubation in the dark at 37℃ or after 1 h incubation in the dark at 37℃ followed by 1 h irradiation with blue light (463 nm) at 25℃ obtained by HPLC-ICP-MS.

Retention time/min[a]	Plasma-dark Area	Ratio/%	Plasma-463 nm Area	Ratio/%
2.75	741	0.50	988	1.038
3.37	0	0	442	0.464
3.64	0	0	15509	16.29
4.51	0	0	26617	27.95
6.18	0	0	6906	7.25
8.84	82	0.055	31325	32.90
11.60	0	0	7064	7.42
14.25	147016	99.44	5934	6.23
17.82	0	0	440	0.462
Sum	147839	100	95226	100

[a] Retention time refers to that in the ^{195}Pt peaks in **Figure S12**. Pt species were extracted from solution using acetonitrile and diluted 10x with MilliQ water.

Table S15. ^{195}Pt signal peak areas of **FM-190** (7756 nM) in plasma or PBS after 1 h incubation in the dark at 37°C followed by 1 h irradiation with blue light (463 nm) at 25°C obtained by HPLC-ICP-MS.

	Plasma-463 nm		PBS-463 nm	
Retention time/min[a]	Area	Ratio/%	Area	Ratio/%
2.75	2045	1.75	1991	2.279
3.26	3135	2.68	366	0.419
3.64	6556	5.60	11017	12.61
4.01	26091	22.27	2625	3.004
4.54	0	0	1215	1.391
4.79	13869	11.84	1699	1.945
5.95	0	0	1417	1.622
8.84	30446	26.00	28511	32.63
9.84	3165	2.70	0	0
10.74	3042	2.60	8002	9.159
11.59	9265	7.91	8034	9.196
13.03	1398	1.19	0	0
14.25	11340	9.68	20505	23.47
15.17	4140	3.53	0	0
16.39	0	0	1129	1.292
17.87	2640	2.25	858	0.982
Sum	117132	100	87369	100

[a] Retention time refers to that in the ^{195}Pt peaks in **Figure S11**. Pt species were extracted from solution by centrifugal filter unit (MWCO 5000) and diluted 10x with MilliQ water.

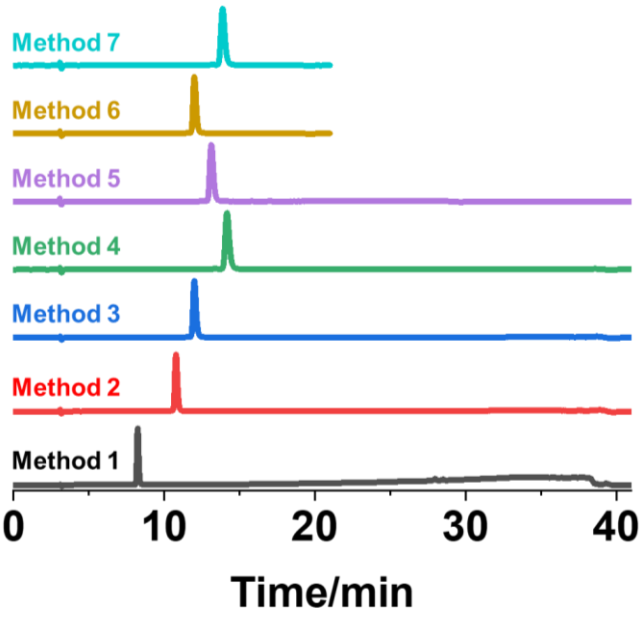

Figure S1. HPLC-UV chromatograms for **FM-190** in MilliQ water in the dark obtained using methods 1-7 (**Table S1**, detection wavelength 254 nm).

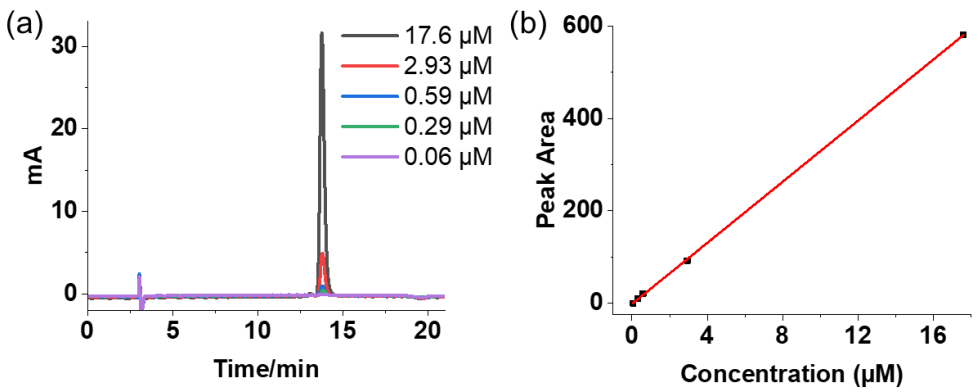

Figure S2. (a) HPLC-UV chromatograms for **FM-190** at increasing concentrations using method-7 (detection wavelength 254 nm); (b) relationship between concentration of **FM-190** and HPLC-UV peak area at 13.8 min, $r^2 = 0.999$.

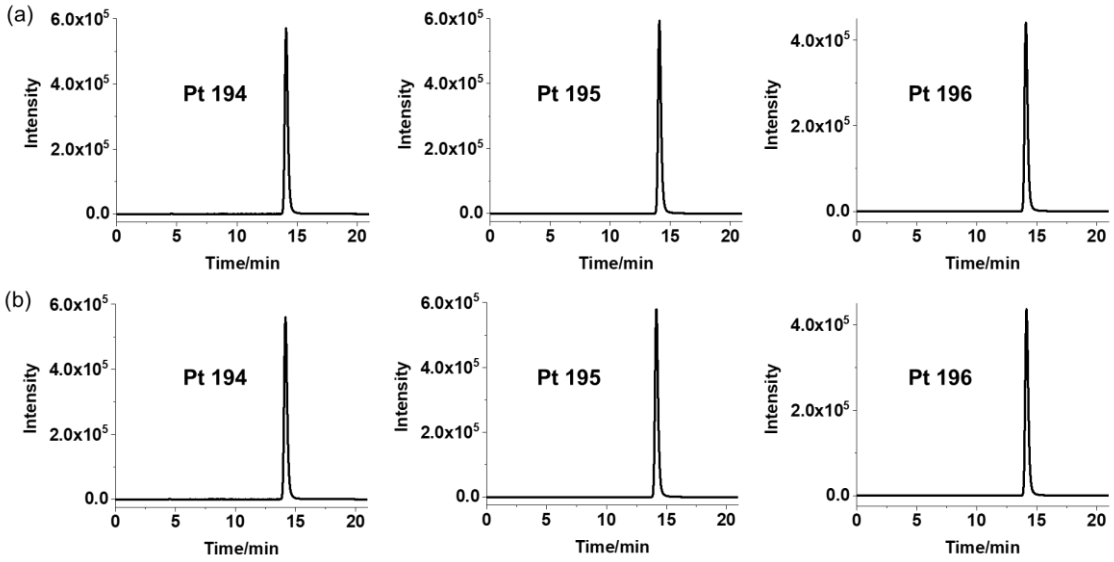

Figure S3. (a) ^{194}Pt, ^{195}Pt, and ^{196}Pt signals of **FM-190** in MilliQ water in the dark obtained by HPLC-ICP-MS; and (b) repetition under same conditions.

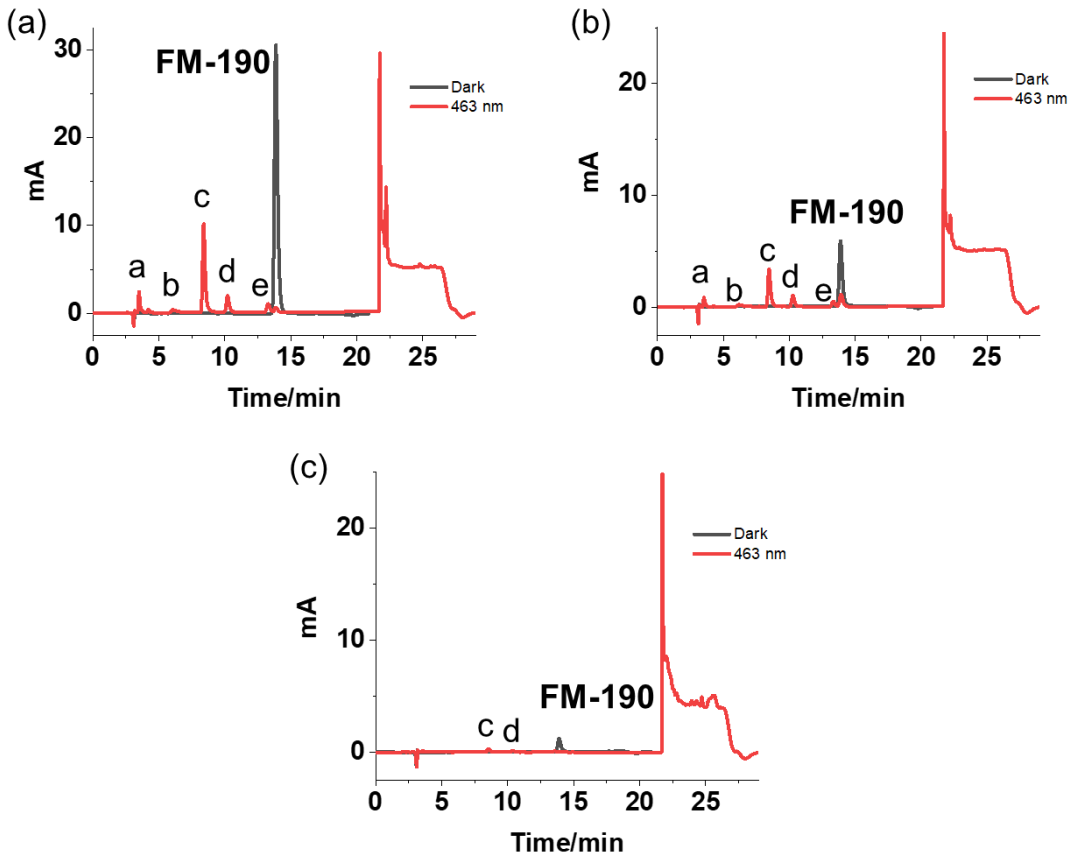

Figure S4. HPLC-UV signals of **FM-190** in MilliQ water obtained using method-7 for dark samples and method-8 for photoactivated samples (463 nm, 1 h, detection wavelength 254 nm) at a concentration of (a) 31.8; (b) 6.4; and (c) 1.3 µM. Species a-e are assigned in **Table S5**.

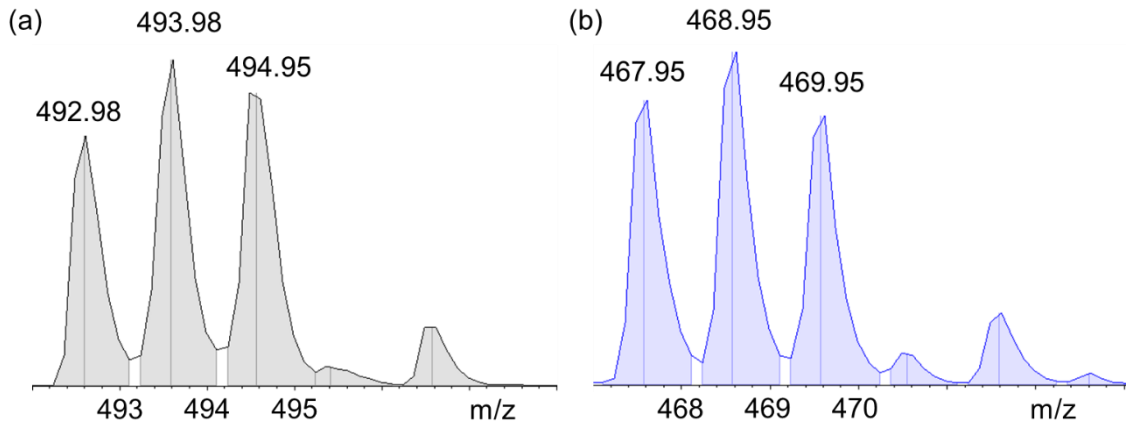

Figure S5. Mass spectra of (a) **FM-190**+Na^+ and (b) photoproduct **c** [{$Pt^{IV}(py)_2(N_3)(OH)_3$}+Na]$^+$ in **Table S5** determined by LC-MS.

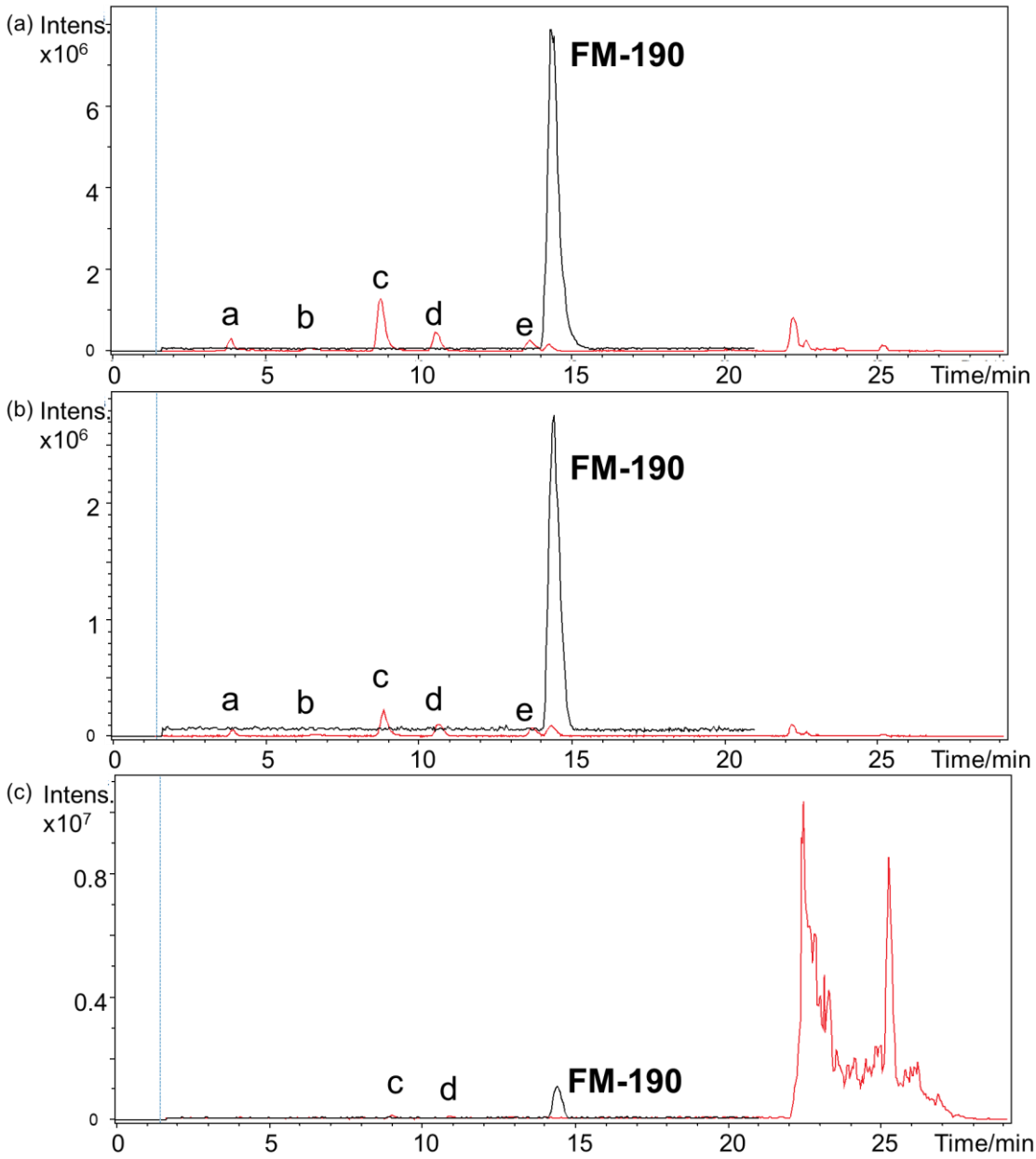

Figure S6. LC-MS chromatogram for **FM-190** in MilliQ water obtained using method-7 for dark samples (—) and method-8 (—) for photoactivated samples (463 nm, 1 h) at a concentration of (a) 31.8; (b) 6.4; and (c) 1.3 µM. Species a-e are assigned in **Table S5**.

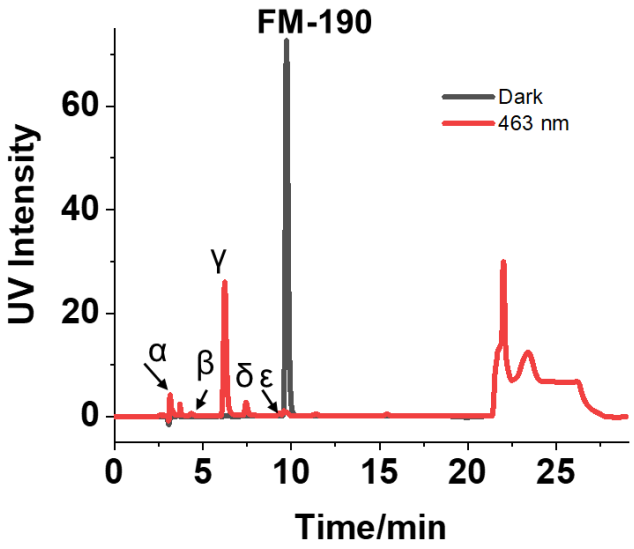

Figure S7. HPLC-UV signals for **FM-190** in MilliQ water obtained using method-9 for dark samples and method-10 for photoactivated samples (463 nm, 1 h, detection wavelength 254 nm) at a concentration of 50 µM. Species α-ε are assigned in **Table S7**.

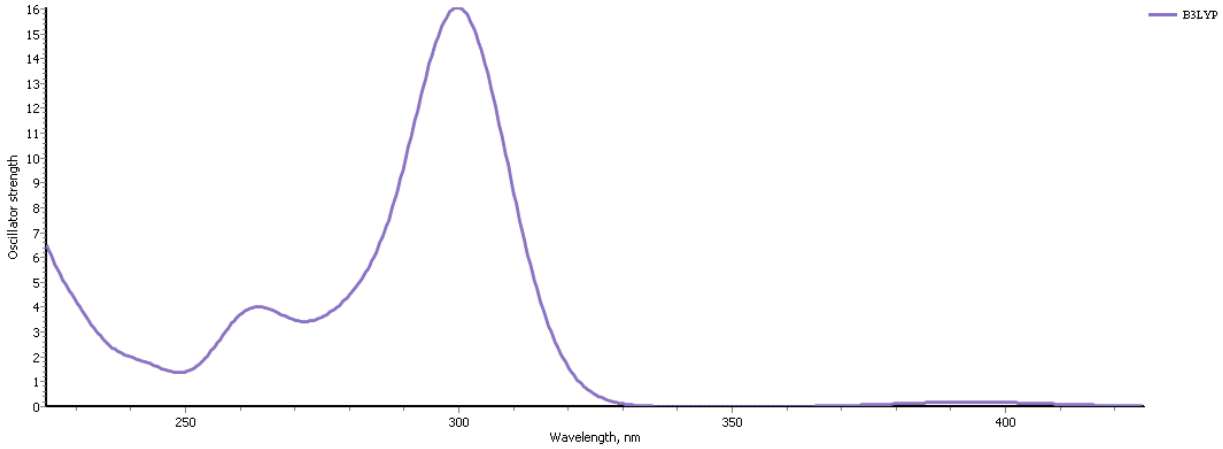

Figure S8. B3LYP computed absorption spectra of **FM-190**.

FM-190	**S1 (nm)**	**S2 (nm)**	**S3 (nm)**
Particle	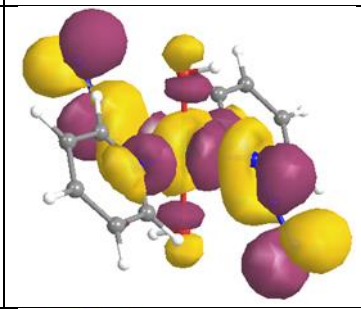	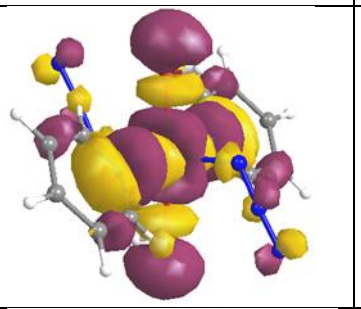	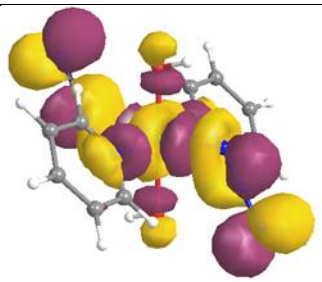
Hole	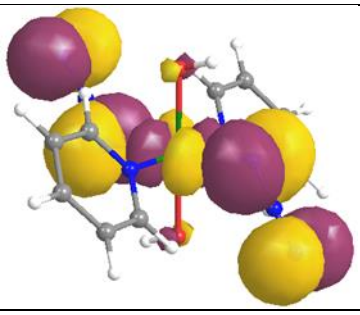	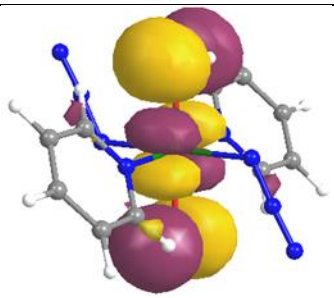	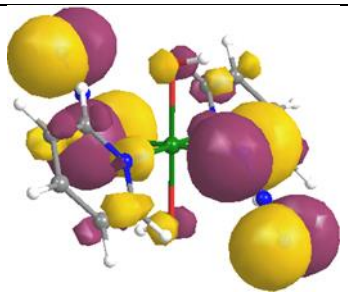

Figure S9. NTOs for **FM-190** singlet states: S1, S2 and S3.

FM-190	T1 (549 nm)	T2 (451 nm)	T3 (449 nm)
Particle	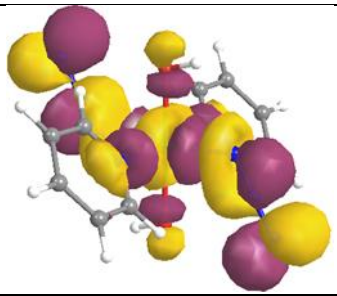	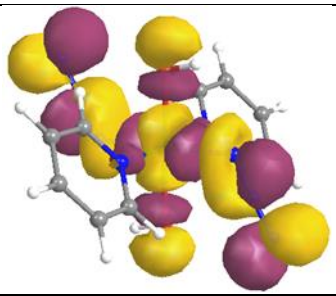	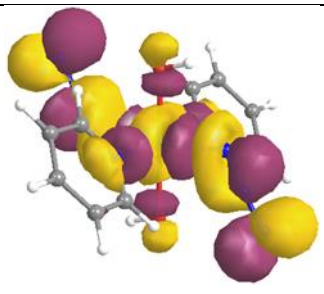

Hole	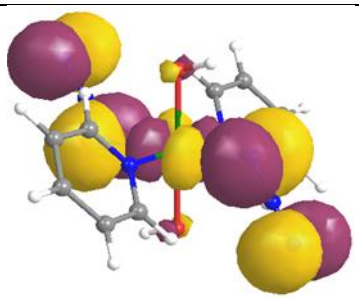	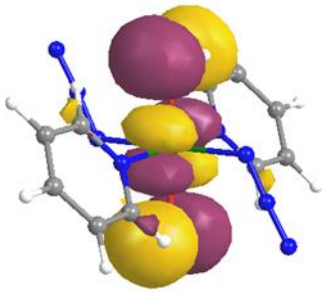	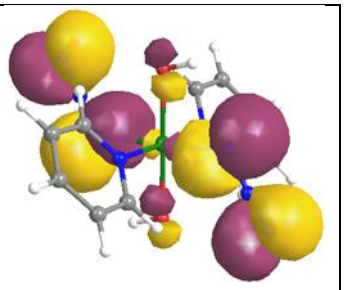
	T4 (437 nm)	T5 (407 nm)	
Particle	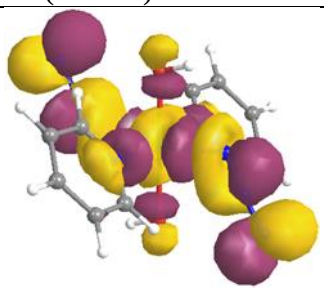	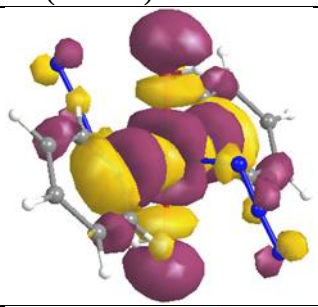	
Hole	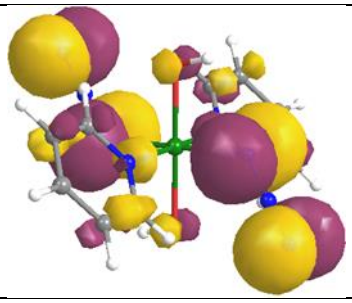	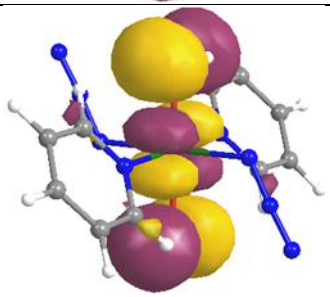	

Figure S10. NTOs for **FM-190** triplet states: T1, T2, T3, T4 and T5.

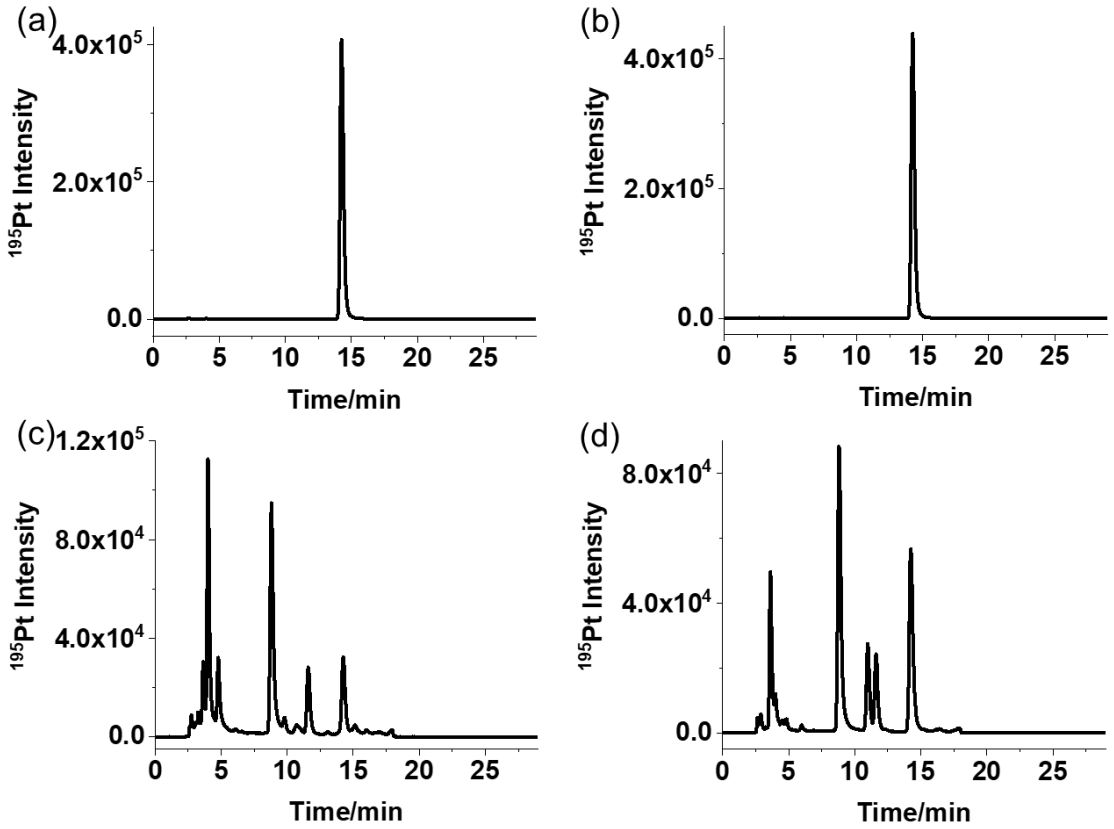

Figure S11. ^{195}Pt signals for **FM-190** in (a) human plasma, or (b) PBS after 2 h incubation in the dark at 37°C, and in (c) human plasma or (d) PBS after 1 h incubation in the dark at 37°C followed by 1 h irradiation with blue light (463 nm) at 25°C. Photoproducts were extracted from the matrix by using a centrifugal filter unit (MWCO 5,000) and diluted 10x with MilliQ water.

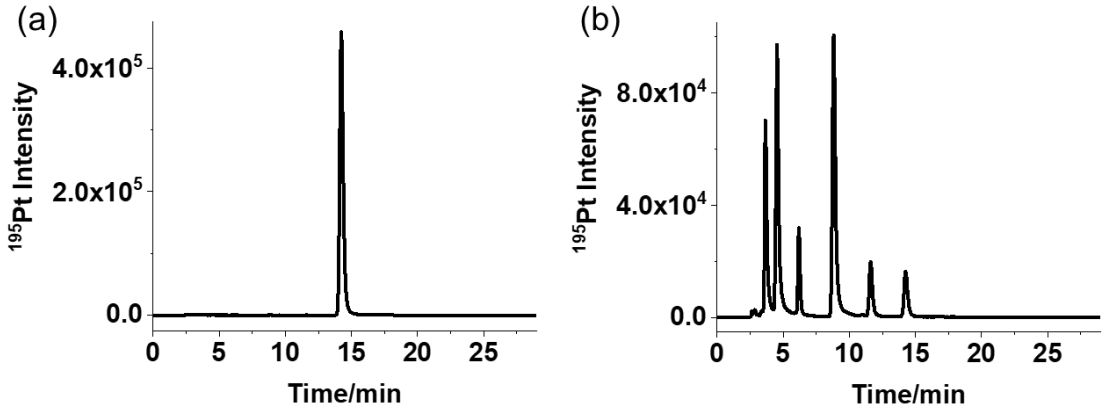

Figure S12. ^{195}Pt signals for **FM-190** in human plasma (a) after 2 h incubation in the dark at 37°C; and (b) after 1 h incubation in the dark at 37°C followed by 1 h irradiation with blue light (463 nm) at 25°C. Photoproducts were extracted from the matrix using acetonitrile and diluted 10x with MilliQ water.

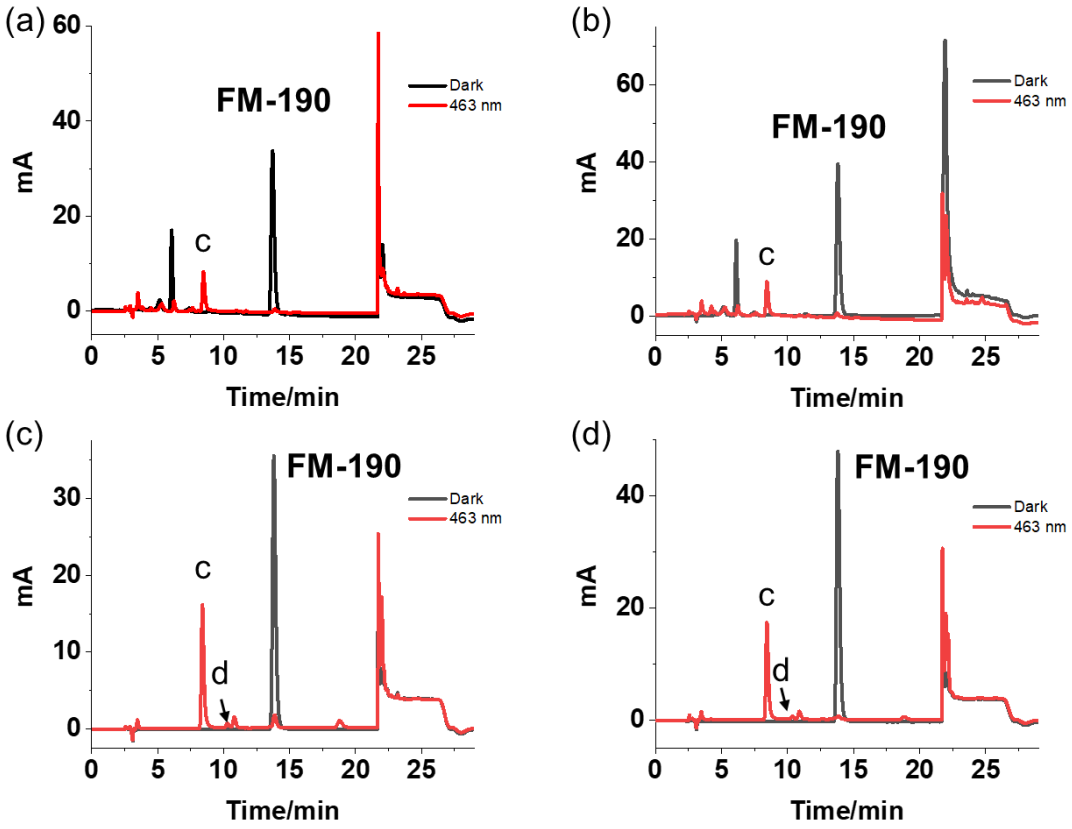

Figure S13. LC-UV signals of **FM-190** (194.9 µM) in human plasma (a and b) or PBS (c and d) after 2 h incubation in the dark at 37°C or after 1 h incubation in the dark at 37°C followed by 1 h irradiation with blue light (463 nm) at 25°C (detection wavelength 254 nm). Photoproducts were extracted from the matrix by centrifugal filter unit (MWCO 5000, a and c) or using acetonitrile (b and d) and diluted 5x with MilliQ water. Species **c** and **d** are assigned in **Table S5**.

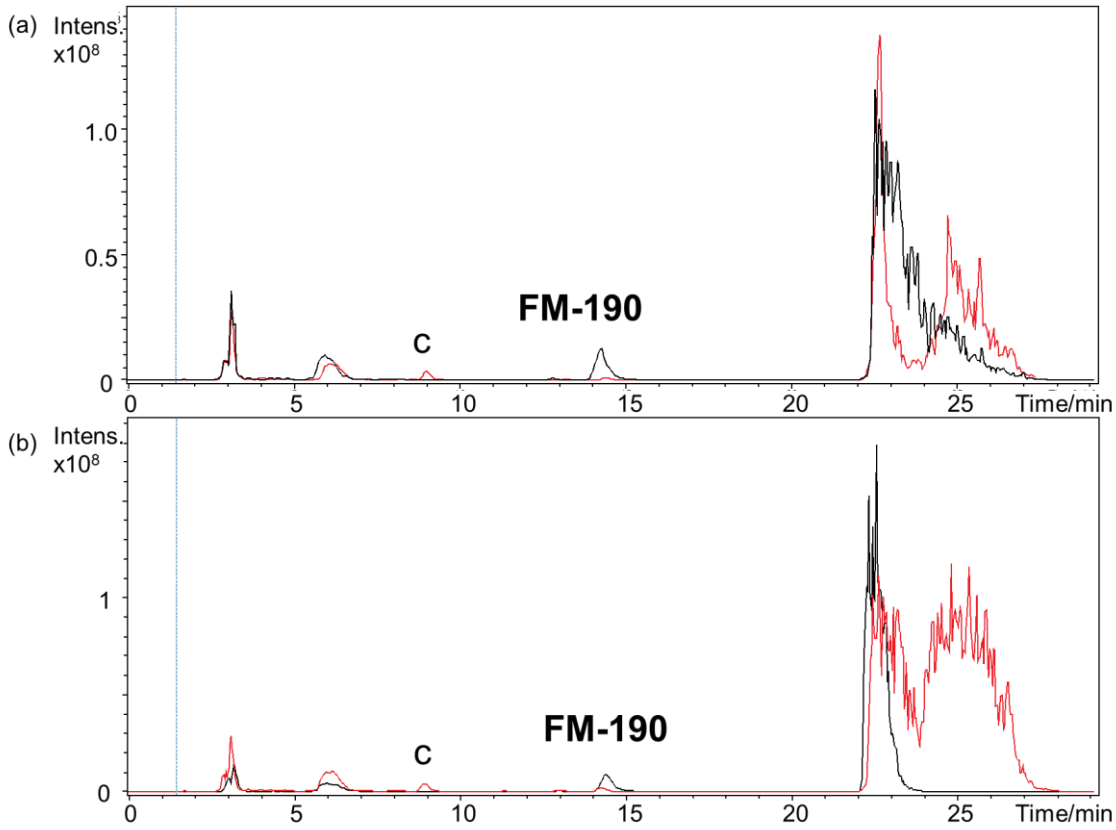

Figure S14. LC-MS chromatogram (BPC+ all MS) of **FM-190** in human plasma after 2 h incubation in the dark at 37°C (—) or after 1 h incubation in the dark at 37°C followed by 1 h irradiation with blue light (463 nm, —) at 25°C. Pt species were extracted from the matrix by (a) centrifugal filter unit (MWCO 5000) or using (b) acetonitrile and diluted 5x with MilliQ water. Species **c** is assigned in **Table S5**. Peaks not labelled are from plasma, suggesting the high stability of **FM-190** in the dark and its ability to release Pt species, some of which might react with components of plasma.

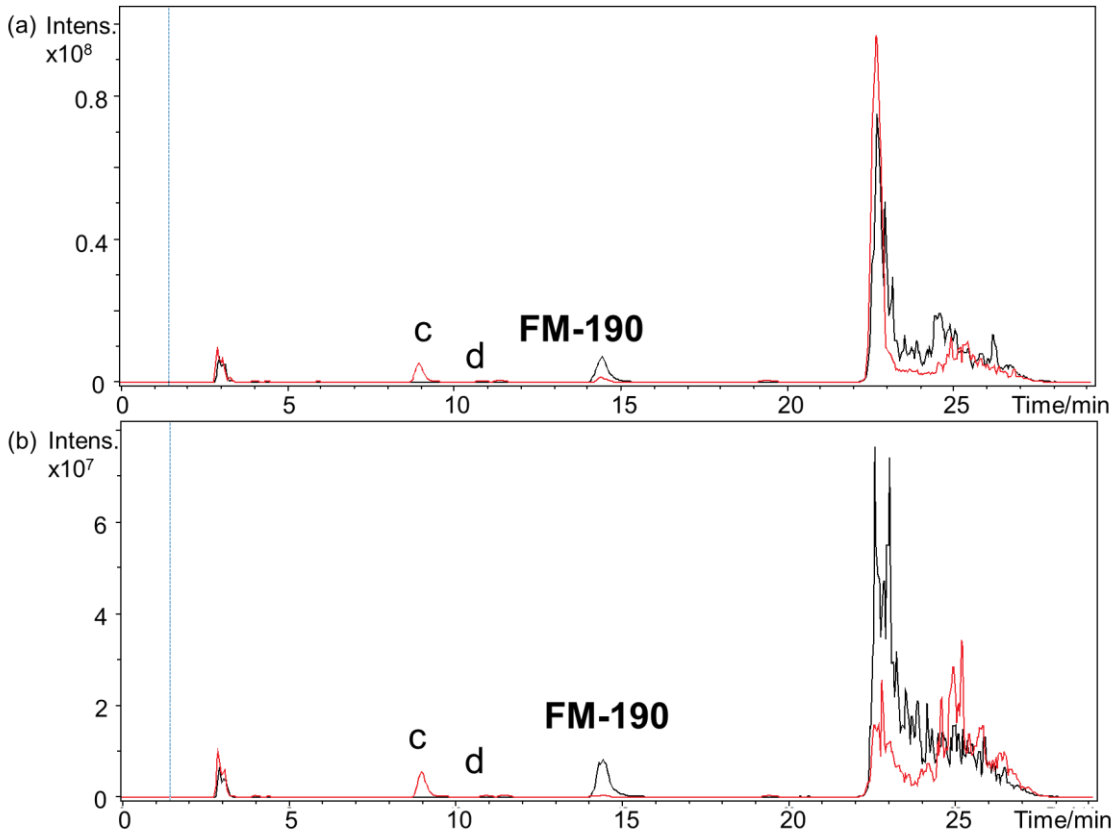

Figure S15. LC-MS chromatogram (BPC+ all MS) of **FM-190** in in PBS after 2 h incubation in the dark at 37°C (—) or after 1 h incubation in the dark at 37°C followed by 1 h irradiation with blue light (463 nm, —) at 25°C. Pt species were extracted from the matrix by (a) centrifugal filter unit (MWCO 5000) or using (b) acetonitrile and diluted 5x with MilliQ water. Species **c** and **d** are assigned in **Table S5**. Peaks not labelled are from PBS, suggesting the high stability of **FM-190** in the dark and its ability to release Pt species.

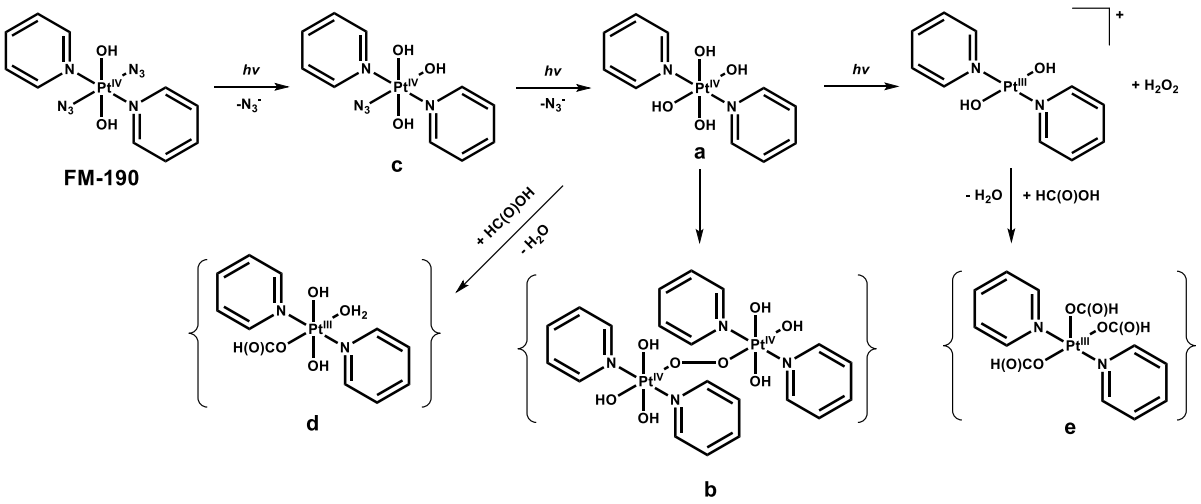

Figure S16. A possible photoactivation pathway for **FM-190** in aqueous solution with blue light (463 nm) irradiation. Species **a-d** and **FM-190** were determined in mass spectrometry as adducts with Na^+, while **e** is an adduct with H^+. Curly brackets are used to denote intermediates that might be formed in the mass spectrometer. The sterochemistries of the photoproducts were not determined in this work.

References

1 N. J. Farrer, J. A. Woods, L. Salassa, Y. Zhao, K. S. Robinson, G. Clarkson, F. S. MacKay, P. J. Sadler, *Angew. Chem. Int. Ed.*, 2010, **49**, 8905–8908.

2 E. Mccurdy, T. Kanda, K. Yamanaka, Y. Chen, and J. Takahashi, Agilent ICP-MS J., 2011, 48, 4–5.

3 D. P. Bishop, D. J. Hare, D. Clases and P. A. Doble, *Trends Anal. Chem.*, 2018, **104**, 11–21.

4 L. H. Møller, C. S. Jensen, T. T. T. N. Nguyen, S. Stürup and B. Gammelgaard, *J. Anal. At. Spectrom.*, 2015, **30**, 277–284.

5 M. J. Frisch, G. W. Trucks, H. B. Schlegel, G. E. Scuseria, M. A. Robb, J. R. Cheeseman, G. Scalmani, V. Barone, G. A. Petersson, H. Nakatsuji, X. Li, M. Caricato, A.V. Marenich, J.Bloino, B. G. Janesko, R. Gomperts, B. Mennucci, H. P. Hratchian, J. V. Ortiz, A. F. Izmaylov, J. L. Sonnenberg, D. Williams-Young, F. Ding, F. Lipparini, F. Egidi, J. Goings, B. Peng, A. Petrone, T. Henderson, D. Ranasinghe, V. G. Zakrzewski, J. Gao, N. Rega, G. Zheng, W. Liang, M. Hada, M. Ehara, K. Toyota, R. Fukuda, J. Hasegawa, M. Ishida, T. Nakajima, Y. Honda, O. Kitao, H. Nakai, T. Vreven, K. Throssell, J. A. Montgomery Jr., J. E. Peralta, F. Ogliaro, M. J. Bearpark, J. J. Heyd, E. N. Brothers, K. N. Kudin, V. N. Staroverov, T. A. Keith, R. Kobayashi, J. Normand, K. Raghavachari, A. P. Rendell, J. C. Burant, S. S. Iyengar, J. Tomasi, M. Cossi, J. M. Millam, M. Klene, C. Adamo, R. Cammi, J. W. Ochterski, R. L. Martin, K. Morokuma, O. Farkas, J. B. Foresman, D. J. Fox, *GaussView 5.0. Wallingford, E.U.A.* 2016.

6 C. Lee, W. Yang, R. G. Parr, *Phys Rev B*, 1988, **37**, 785–789.

7 A. D. Becke, *J. Chem. Phys.*, 1993, **98**, 5648–5652.

8 S. Grimme, J. Antony, S. Ehrlich and H. Krieg, *J Chem Phys*, 2010, **132**, 154104.

9 D. Andrae, U. Häußermann, M. Dolg, H. Stoll and H. Preuß, *Theoret. Chim. Acta*, 1990, **77**, 123–141.

10 A. V. Marenich, C. J. Cramer and D. G. Truhlar, *J. Phys. Chem. B*, 2009, **113**, 6378–6396.

11 T. Yanai, D. P. Tew and N. C. Handy, *Chem. Phys. Lett.*, 2004, **393**, 51–57.

12 M. Ernzerhof and G. E. Scuseria, *J. Chem. Phys.*, 1999, **110**, 5029–5036.

13 C. Adamo and V. Barone, *J. Chem. Phys.*, 1999, **110**, 6158–6170.

14 Y. Zhao, N. E. Schultz, D. G. Truhlar, *J. Chem. Phys.* 2005, **123**, 161103.

15 Y. Zhao and D. G. Truhlar, *Theor. Chem. Acc.*, 2008, **120**, 215–241.

16 Y. Zhao and D. G. Truhlar, *J. Chem. Phys.*, 2006, **125**, 194101.

17 D. Escudero and W. Thiel, *J. Chem. Phys.*, 2014, **140**, 194105.

18 D. Escudero, E. Heuser, R. J. Meier, M. Schäferling, W. Thiel and E. Holder, *Chem. Eur. J.*, 2013, **19**, 15639–15644.

19 F. Neese, *Wiley Interdiscip. Rev. Comput. Mol. Sci.*, 2012, **2**, 73–78.

20 F. Neese, *Wiley Interdiscip. Rev. Comput. Mol. Sci.*, 2018, **8**, e1327.

21 K. Fukui, *J. Phys. Chem.*, 1970, **74**, 4161.

22 C. Gonzalez and H. Bernhard Schlegel, *J. Chem. Phys.*, 1989, **90**, 2154–2161.